ChemComm

Negative thermal quenching of photoluminescence in a copper–organic framework emitter

Journal:	*ChemComm*
Manuscript ID	CC-COM-07-2020-004788.R2
Article Type:	Communication

ChemComm

COMMUNICATION

Negative thermal quenching of photoluminescence in a copper–organic framework emitter

Received 00th January 20xx,
Accepted 00th January 20xx

DOI: 10.1039/x0xx00000x

www.rsc.org/

Ting Wu,[a,§] Shenlong Jiang,[b,§] Pabitra Narayan Samanta,[c,§] Yangbin Xie,[a] Jipeng Li,[a] Xiaoling Wang,[a] Devashis Majumdar,[c] Xiangwei Gu,[a] Yusong Wang,[b] Wei Huang,[a] Qun Zhang,[b,*] Jerzy Leszczynski[c,*] & Dayu Wu[a,*]

ABSTRACT: Negative thermal quenching (NTQ), an abnormal phenomenon that the intensity of photoluminescence (PL) increases with increasing temperature, has essentially been restricted to either bulk semiconductors or very low temperatures. Here, we report a delayed fluorescence copper–organic framework exhibiting negative thermal quenching (NTQ) of photoluminescence, which is driven by the fluctuation between localized and delocalized form of its imidazole ligand. The process is completely reversible on cooling/heating cycles. This study opens a new avenue to explore the electronically switchable NTQ effect in coordination networks and further to develop the NTQ-based light-emitting diodes.

The integrated intensity of the photoluminescence (PL) in solids, such as semiconductors and molecular crystals, would normally decrease monotonically with increasing temperature[1]. The phenomenon is called thermal quenching (TQ) due to the rapid increase of nonradiative relaxation of excited electrons to the ground state with increasing temperature[2]. Such a TQ effect severely influences the efficiency and degrades the performance of the light-emitting diodes. Therefore, developing photoluminescent materials that are against TQ is of great practical significance[3]. In some semiconductor nanostructures, such as ZnO and CdSe, however, the PL intensity increases with increasing temperature[4–6]. This abnormal phenomenon is termed negative thermal quenching (NTQ) of PL, which frequently occurs at very low temperatures (*i.e.* several tens of Kelvin) in conventional semiconductors. To explore the potential of molecular-based NTQ at room temperature (RT), it is essential to investigate the structural origins that differ from nanostructures in related characteristics[7]. An inherent challenge to the elaboration of NTQ effect in molecular-based materials is the requisite rearrangement of molecular or electronic structures under external thermal stimulus within a crystalline-state matrix for effective transformation from TQ to NTQ akin to the classical definition[8,9]. Thermally activated delayed fluorescence (TADF) provides a potential strategy for the design of molecular NTQ systems by virtue of the thermally activated singlet harvesting mechanism[10,11]. However, the TADF-type emitters frequently suffer from TQ because of the radiationless deactivation[12–16]. So far, quite limited examples are known, and the control of responsive electronic states at atomic level in TADF emitters remains hypothetical[17, 18].

In this work, we report a precise control of NTQ effect in a TADF-type copper(I) iodide metal–organic layered framework, **bibeCu$_4$I$_4$**, through thermally driven transition between two distinct electronic structures. Temperature-dependent X-ray diffraction, *in-situ* infrared, Raman and solid-state NMR spectra reveal an unprecedented electronic structure consisting of atomically resolved entanglement of localized and delocalized electronic structures of imidazole ligand, which can be manipulated to tune the temperature dependence of PL[19]. The pronounced NTQ effect occurs concomitantly with the electronic structural transition and the PL intensity reaches the maximum at 260 K. Considering both the structural and electrostatic effects during the radiative and nonradiative electron transfer processes, first-principle based approaches validate the genesis of NTQ luminescence and mechanism of TADF in the copper–organic framework. The current investigation sheds new light on the understanding of NTQ effect associated with the entangled electronic structure in molecular-based materials.

Single-crystal X-ray diffraction analysis reveals that the compound crystallizes in the monoclinic $P2_1/n$ space group (ESI Table 1). The asymmetric unit consists of two crystallography-independent Cu(I) ions and two I^- anions plus half organic linker centered on the

[1]Jiangsu Key Laboratory of Advanced Catalytic Materials and Technology, Advanced Catalysis & Green Manufacturing Collaborative Innovation Center, School of Petrochemical Engineering, Changzhou University, Changzhou, Jiangsu 213164, P. R. China. E-mail: wudy@cczu.edu.cn
[2]Hefei National Laboratory for Physical Sciences at the Microscale, Department of Chemical Physics, Synergetic Innovation Center of Quantum Information & Quantum Physics, University of Science and Technology of China, Hefei, Anhui 230026, P. R. China. E-mail:qunzh@ustc.edu.cn (Q. Z.);
[3]Interdisciplinary Center for Nanotoxicity, Department of Chemistry and Biochemistry, Jackson State University, MS – 39217, USA. E-mail: jerzy@icnanotox.org (J. L.)
§These authors contributed equally to this work.

† Electronic supplementary information (ESI) available. CCDC 1975148, 1975149 and 1975151–1975155. For ESI and crystallographic data in CIF or other electronic format see DOI: 10.1039/x0xx00000x.

inversion center (Fig. 1a). Both tetrahedral Cu(I) ions and two iodines comprise a [Cu_2I_2] rhombic plane with a small average deviation (0.087 Å) and the shortest Cu···Cu interaction of 2.844(5) Å at 80 K, which shows a linear increment with temperature (ESI Fig. 2). The [Cu_2I_2] rhomboid transforms into a ribboned topology along the crystallographic *b* direction, which can be described as a shoulder-by-shoulder arrangement of four zigzag CuI chains of {CuI_4}/{CuI_3N} edge-shared tetrahedra. The imidazole-based ligand, bibe, serves as the bridge and isolates the one-dimensional (1D) CuI ribbons with a diameter of 0.66 nm in a 2D metal–organic layered framework[20] (Fig. 1b).

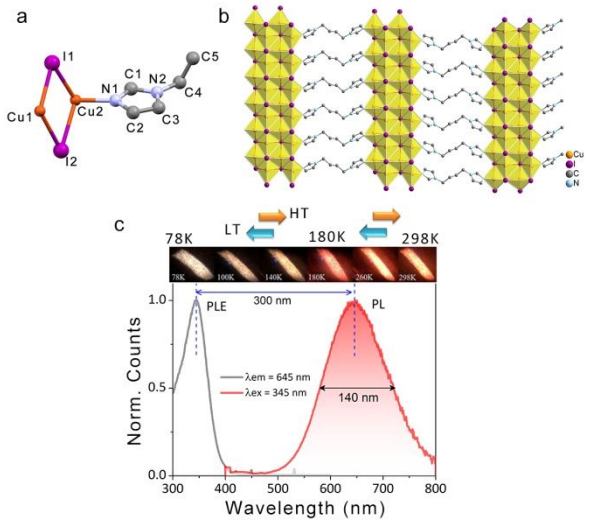

Fig. 1 (a) The asymmetric unit of the compound, **bibeCu$_4$I$_4$**, in a ball-and-stick style. The color system: Cu (red), I (purple), N (blue) and C (gray). All hydrogen atoms are not shown for clarity. (b) The polyhedron representation of 1D copper iodide ribbons of edge-sharing {CuI_4}/{CuI_3N} tetrahedra. (c) PL excitation (PLE, blue) and PL (red) spectra of **bibeCu$_4$I$_4$** crystals at 298 K. The top panel in (c) shows PL photos of **bibeCu$_4$I$_4$** microcrystal in the temperature range of 78–298 K.

The experimental and simulated electronic absorption spectra of **bibeCu$_4$I$_4$** structural motif are investigated (ESI Fig. 3,4). The calculated vertical excitation energies (E_{ex}), oscillator strengths (f), dipole strengths (S), and major contributions of the molecular orbitals (MOs) for the electronic excitations with $f > 0.05$ are provided in (ESI Table 2). The analysis of electron density distributions of frontier molecular orbits (MOs) contributing low-lying singlet-singlet excited states (ESI Fig. 5) indicates that the absorption band in the UV region crucially emanates from the electronic transitions involving the MOs localized on the [Cu_4I_4] cluster comprised of $3d$-orbitals of Cu(I) atom and $5p$-orbitals of the coordinating I atoms as well as the **bibe** ligand-centered π^* orbital. The **bibeCu$_4$I$_4$** crystalline sample exhibits a broad PL spectrum with a full width at half maximum (FWHM) of 140 nm, a large Stokes shift of 300 nm (Fig. 1c) and the Commission Internationale d'Eclairage (CIE) coordinate of (0.57, 0.42) at room temperature. The emission spectra are broad and featureless with a peak of 645 nm at 298 K. DFT calculated vibrationally resolved emission spectra indicate that the wide emission band includes the superposition of two components, *i.e.*, the spin-allowed $S_1 \rightarrow S_0$ (fluorescence) and spin-forbidden $T_1 \rightarrow S_0$ (phosphorescence) transitions, with the singlet–triplet separation of 0.17 eV (ESI Fig. 6).

The visually impressive brightening luminescence of **bibeCu$_4$I$_4$** is evidenced upon heating the crystals from cryogenic temperature to RT under UV light (ESI Movie). No fatigue or degradation is observed by naked eye after many tens of cooling/heating cycles. Such a type of negative thermal quenching of PL is reminiscent of conventional semiconductor quantum dots (*e.g.*, CdSe, CdTe and PbS)[5,6,21–23]. However, the full understanding of mechanism behind should involve the structural analysis at atomic level in molecular-based materials. The *in-situ* electronic absorption spectra indicate that the TQ→NTQ transformation in this system possibly originates from the variation of electronic structure under thermal stimulus (ESI Fig. 3b).

To investigate the temperature-dependent emissions of **bibeCu$_4$I$_4$**, the PL spectra in the temperature range of 78–350 K are recorded. The PL spectra of **bibeCu$_4$I$_4$** in this temperature range are plotted in Fig. 2a. The qualitative observation provides the continuous brightening of PL emission when approaching RT, which conforms to the naked-eye detection. The result is counterintuitive and turns out to be a reversible phenomenon after several tens of heating/cooling cycles (Fig. 2b). Fig. 2c (top, circle line) shows the temperature dependence of the integrated PL intensity of **bibeCu$_4$I$_4$**. Upon heating the crystalline sample in the atmosphere of liquid nitrogen, the PL intensity is slightly increased in the low-temperature region (< 180 K) and begins to sharply increase (reaching the maximum at 260 K) and thereafter decreases. At 298 K, the PL intensity still maintains 65% of the maximum intensity with quantum yield of 11.6%[24]. As the temperature increases, the emission band exhibits a continuous shift toward higher energy (ESI Fig. 7), suggesting that the excited electrons tend to populate at a higher vibrational state with increasing temperature[25,26].

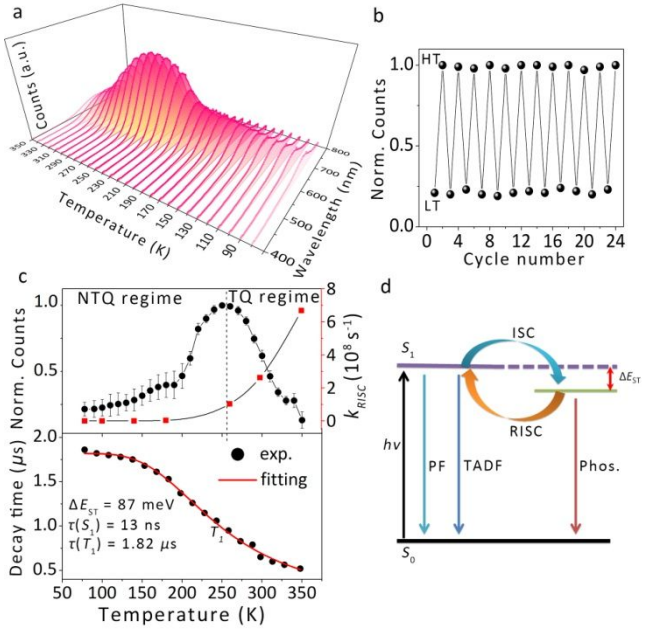

Fig. 2 (a) PL emission spectra of **bibeCu$_4$I$_4$** (λ_{ex} = 345 nm) at different temperatures. (b) The reversible PL change upon many heating/cooling cycles. (c) Top: the integrated PL intensity (circle line) and the simulated RISC rate (square line) as a function of temperature. The error bars are estimated as the respective deviations from five independent measurements, and the average data are recorded. Below: temperature dependence of the decay times for the complex **bibeCu$_4$I$_4$**. The red line is the least-square best fitting result. (d) Schematic of excited-state transitions in **bibeCu$_4$I$_4$**.

To understand the nature of excited states, we conduct temperature-dependent PL decay measurements as shown in Fig. 2c (below)[27]. The fitting results are as follows: $\tau(S_1)$ = 13 ns, $\tau(T_1)$ = 1.82 μs and ΔE_{ST} = 0.087 eV. It should be noted that the $\tau(T_1)$ value is very close to the observed value at 78 K and the ΔE_{ST} value is in good agreement with the value (~0.1 eV) determined from the onsets of the emission spectra recorded at 78 and 350 K, that matches well with the estimated singlet–triplet energy splitting of

0.17 eV from DFT calculations. On the basis of excited state geometries and emission energies within the framework of SS-TD-DFT, the radiative lifetimes are computed as the inverse of the Einstein spontaneous emission coefficient. The intrinsic decay times for the S_1 and T_1 states are estimated to be 22.34 ns and 1.02 µs, respectively, that compares well with the experimental PL decay data. The small ΔE_{ST} is comparable to those of the efficient TADF-type Cu(I) compounds[28–32].

To unveil the fundamental mechanism of TADF, we emphasize on the estimations of radiative and nonradiative rate constants of photoexcited electron transfer processes through the exploration of photophysical properties of low-lying singlet and triplet excited states on the potential energy hypersurface. Within the framework of semiclassical Marcus theory, the rate of $T_1 \rightarrow S_1$ up-conversion is calculated to be 3.15×10^8 s^{-1}, which is 3 orders of magnitude faster than the phosphorescence rate ($k_{phos} = 9.77 \times 10^5$ s^{-1}). The RISC rate also appears to be comparable to the radiative decay rate of the S_1 state of 4.48×10^7 s^{-1}. Therefore, a rapid equilibrium between the rates of populations of S_1 and T_1 states could be achieved before decaying radiatively at room temperature. The PL efficiency is promoted by the faster RISC rate after thermal equilibrium when temperature exceeds 260 K, as depicted in Fig. 2c (top, square line), leading to the emergence of NTQ effect. Furthermore, the distortion motion of the [Cu_4I_4] structural units render effective pathway for the interconversion of $T_1 \rightarrow S_1$ as revealed by the excited-state dynamics simulation that incorporates electron–phonon and spin-mixing interactions. Consequently, the triplet T_1 reservoir can transit efficiently into the S_1 state with increasing temperature, giving rise to a very pronounced shortening of the TADF decay time when compared to the previous copper complexes (*i.e.*, several to tens of microsecond) (Fig. 2d).

In order to understand the structural origin of the spectral response, the X-ray diffraction data are collected on a single crystal from 80 to 298 K (with an interval of 40 K) in the atmosphere of liquid nitrogen. As shown in Fig. 3a, all the bond distances below 260 K, including C–N and C–C bonds, in the imidazole ring, are approximately equal and fall within the range between normal double and single bonds, which indicates that the observed structure is a superposition of the unresolved resonance structures[19,33]. However, above 260 K, some bond distances, *i.e.*, C1–N1 and C2–C3, begin to decrease; in contrast, the bond elongation occurs for the remaining bonds, especially for C3–N2. This result indicates excess heat energy drives the electronic structural transiton of the imidazole ring. The characteristic peaks assignable to the imidazole ring are also observed to change in the *in-situ* FT-IR and Raman spectra at the temperature where the possible electron localization of imidazole ring occurs (Fig. 3b,c and ESI Fig. 8,9).

The variable-temperature solid-state ^{13}C NMR spectra further provide useful information on the electronic structure, as shown in Fig. 3d. At 187 K, five sharp chemical-shift peaks at approximately 49.6, 118.4, 127.2, 130.4 and 140.6 ppm are assigned to C4, C3, C5, C2 and C1, respectively. Such sharp and strong NMR signals originate from the conjugate effect of the imidazole ring. As the temperature approaches 250 K, the imidazole ring begins to evidence the electronic perturbation, which leads to the weakening of the ring current shielding effect and hence the broadening of the NMR profiles[34]. At 300 K, the imidazole ring becomes a localized structure and hence some peaks, such as C2 and C3, show the down-field shift and become sharpened again. The relevant details are collected (ESI Fig. 10). Notably, the unusual enhancement of NMR signals of C2 and C4 at 187 K provides a hint of the specific directional configuration in the imidazole ring. This observation clearly reveals the thermally induced delocalization-to-localization transition in the imidazole ring (Fig. 3e). This phenomenon of NTQ effect in the temperature range of 78–260 K originates from the ability of the TADF emitter to suppress the emission losses and thus increase the PL with increasing temperature. However, this situation no longer holds above 260 K because the localized form of imidazole ring begins to emerge at 260 K. This observation demonstrates that the ligand's electronic structure play a crucial role in the temperature dependence of PL in the luminescent copper complex[35].

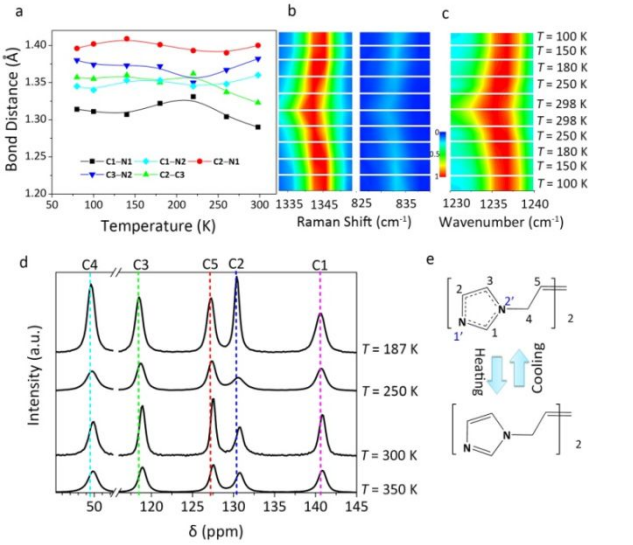

Fig. 3 (a) Temperature-dependent bond distances of imidazole ligand. (b) Temperature-dependent Raman and (c) IR spectra of **bibeCu$_4$I$_4$** in the selected bands upon cooing from RT to 100 K, and subsequent heating to RT. (d) The ^{13}C NMR spectra recorded at different temperatures. The colored dashed lines are the guide for eye. (e) Reversible thermally induced electronic switching of imidazole ring in copper–organic framework.

In the femtosecond time-resolved transient absorption (fs-TA) spectra, the excitation energy (340 nm, or 3.65 eV) that induces S_1 excitation is consistent with that in the PL measurements[36]. The white-light continuum probe (500–800 nm) turns out to yield essentially the same spectral profiles for **bibeCu$_4$I$_4$** at different temperatures, as displayed in Fig. 4a(top). It is found that the intensity of excited S_1 emission gradually increases in the range of 100–250 K and then decreases in the range of 250–350 K, which nicely echoes to the observation in the temperature-dependent PL spectra (Fig. 2a). Furthermore, by deploying quasi-degenerate perturbation theory (QDPT), the mixing between triplets and singlets derived from TD-DFT has been evaluated to examine the impact of SOC mixing on the rate of nonradiative RISC (ESI Table 3). The computed average SOC value between S_1 and T_1 state is about 21 cm^{-1}, which is significantly enhanced by the heavy-atom effect compared to the purely organic TADF emitters yielding insubstantial SOC value (≤ 1 cm^{-1})[37]. The SOC corrected emission spectrum is delineated in Fig. 4a(below). The apex of emission spectrum appears at 669 nm that coincides with the result obtained by fs-TA spectroscopic technique.

The analysis of relaxation kinetics at different temperatures further confirms the mechanism involving ISC and RISC processes in **bibeCu$_4$I$_4$**, as shown in Fig. 4(b). In the range of 100–150 K, there is no sufficient external heat for activating the T_1 state and thus no obvious stimulated emission from the S_1 state. With increasing temperature, the T_1 state can be thermally activated and subsequently the RISC process results in the delayed fluorescence in

the range of 180–300 K. The shadow region reveals a plateau at the early stage over roughly 18 μs, reflecting an equilibrium is attained between the two inter-convertible excited states. The exponential decay after such an equilibrium stage features a lifetime of roughly 1 μs, corresponding to the process that the T_1 population returns to the ground state *via* the S_1 state. Notably, such a relaxation lifetime is in agreement with that in the PL measurements. Therefore, the fs-TA results as well as DFT calculations not only confirm the PL mechanism of **bibeCu$_4$I$_4$**, but also disclose the ultrafast relaxation dynamics involved in the system.

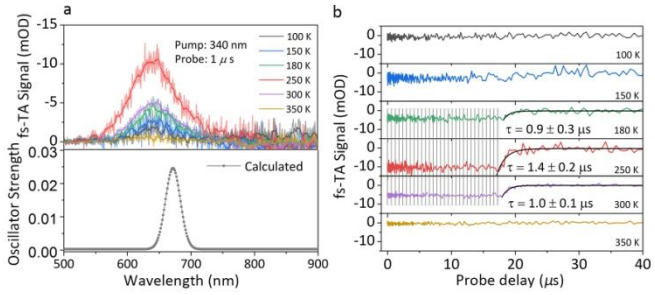

Fig. 4 (a) Top: The temperature-dependent fs-TA spectra of **bibeCu$_4$I$_4$** at the probe delay of 1-μs under 340 nm excitation. The fs-TA signal (*i.e.*, the absorbance change) is given in mOD (OD: optical density). Below: The calculated PL spectrum obtained at the PCM-tuned TD-B3LYP level including the SOC effect by means of QDPT. (b) The corresponding kinetic traces of **bibeCu$_4$I$_4$** taken at each peak of the spectral profile at different temperatures.

In summary, this study described a drastic negative thermal quenching behavior in an electronically dynamic copper(I) metal–organic layer. With increasing temperature, the ligand's electronic delocalization-to-localization transition occurs upon heating. We propose that the temperature dependence of photoluminescence arises from the electronic localization-to-delocalization transition centered on its imidazole ligand, which dictates the final delayed fluorescence intensity. This work provides a fundamental understanding for the development of advanced molecular-based NTQ emitters that can be operative at high temperatures in the field of organic light-emitting diodes. Further improving the efficiency NTQ effect in copper-organic framework emitters by introducing dynamic electronic structure will be reported in due course.

We are thankful for financial support from the PAPD of Jiangsu Higher Education Institutions. This work is supported by the National Natural Science Foundation of China (21671027, 21573211, 21633007, 21803067), the National Key R&D Program of China (2016YFA0200602, 2018YFA0208702), the USTC-NSRL Joint Funds (UN2018LHJJ) and the Anhui Initiative in Quantum Information Technologies (AHY090200). P. N. S., D. M. & J. L. thank the Department of Energy, US (Grant number: DE-SC0018322) for the financial support.

Conflicts of interest

There are no conflicts to declare.

Notes and references

1. D. Di, A. S. Romanov, L. Yang, J. M. Ritchter, J. P. H. Rivett, S. Jones, T. H. Thomas, M. A. Jalebi, R. H. Friend, M. Linnolahti, M. Bochmann and D. Credgington, *Science* 2017, **356**, 159–163.
2. B. Valeur and M. N. Berberan-Santos, *Molecular fluorescence: principles and applications*. Wiley-VCH, Weinheim, 2013.
3. Y. H. Kim, P. Arunkumar, B. Y. Kim, S. Unithrattil, E. Kim, S.-H. Moon, J. H. Hyun, K. H. Kim, D. Lee, J.-S. Lee and W. B. Im, *Nat. Mater.* 2017, **16**, 543−550.
4. M. Watanabe, M. Sakai, H. Shibata, T. Shibayama, H. Tampo, A. Yamada, K. Matsubara and K. Sakurai, *Physica B.* 2006, **376–377**, 711–714.
5. S. F. Wuister, C. de Mello Donegá and A. Meijerink, *J. Am.Chem. Soc.* 2004, **126**, 10397–10402.
6. S. F. Wuister, A. van Houselt, C. de Mello Donegá, D. Vanmaekelbergh and A. Meijerink, *Angew. Chem., Int. Ed*. 2004, **43**, 3029–3033.
7. H. Barkaoui, H. Abid, S. Zelewski, J. Urban, M. Baranowski, A. Mlayah, S. Triki P. Plochocka and Y. Abid, *Adv. Optical Mater*. 2019, **7**, 1900763.
8. V. W. W.Yam, V. K. M. Au, S. Y. L. Leung, *Chem. Rev.* 2015, **115**, 7589–7728.
9. H.Uoyama, K. Goushi, K. Shizu, H. Nomura and C. Adachi, *Nature* 2012, **492**, 234−238.
10. J. R. Kirchhoff, J. R. E. Gamache, M. W. Blaskie, A. A. D. Paggio, K. R. Lengel and D. R. McMillin, *Inorg. Chem*. 1983, **22**, 2380–2384.
11. D. G. Cuttell, S. M. Kuang, P. E. Fanwick, D. R. McMillin, R. A. Walton, *J. Am. Chem. Soc.* 2002, **124**, 6–7.
12. D. Volz, Y. Chen, M. Wallesch, R. Liu, C. Fléchon, D. M. Zink, J.Friedrichs, H. Flügge, R. Steininger, J. Göttlicher, C. Heske, L.Weinhardt, S. Bräse, F. So and T. Baumann, *Adv. Mater*. 2015, **27**, 2538–2543.
13. M. J. Leitl, V. A. Krylova, P. I. Djurovich, M. E. Thompson and H. Yersin, *J. Am. Chem. Soc*. 2014, **136**, 16032−16038.
14. J. C.Deaton, S. C.Switalski, D. Y. Kodakov, R. H. Young, T. D. Pawlik, D. J. Giesen, S. B. Harkins, A. J.M. Miller, S. F. Mickenberg and J. C. Peters, *J. Am. Chem. Soc*. 2010, **132**, 9499–9508.
15. T. Hofbeck, U. Monkowius and H. Yersin, *J. Am. Chem. Soc*. 2015, **137**, 399−404.
16. L. Bergmann, G. J. Hedley, T. Baumann, S. Bräse and I. D. W. Samuel, *Sci. Adv*. 2016, **2**, e1500889.
17. R. Hamze. R. Peltier, J. L. Sylvinson, D. Jung, M. Cardenas, J. Haiges, R. Soleilhavoup, M. Jazzar, R. Djurovich, P. I. Bertrand, G.Thompson and E. Mark, *Science* 2019, **363**, 601–606.
18. L. L.-M. Zhang, G. Zhou, G. Zhou, H.-K. Lee, N. Zhao, O. V. Prezhdo and T. C. W. Mak, *Chem. Sci.* 2019, **10**, 10122−10128.
19. C. Curutchet, J. Poater, M. Solà, J. Elguero, *J. Phys. Chem. A* 2011, **115**, 8571–8577.
20. R. Y. Wang, X. Zhang, Q. F. Yang, Q. S. Huo, J. H. Yu, J. N. Xu and J. Q. Xu, *J. Solid State Chem*. 2017, **251**, 176–185.
21. P. T. Jing, *J. Phys. Chem. C* 2009, **113**, 13545−13550.
22. A. M.Jagtap, J. Khatei and K. S. R. K. Rao, *Phys. Chem. Chem. Phys*. 2015, **17**, 27579−27587.
23. L. Turyanska, A. Patane, M. Henini, B. Hennequin and N. R. Thomas, *Appl. Phys. Lett*. 2007, **90**, 101913.
24. The absolute quantum yield is determined through a direct method using a quantum yield measurement system provided by Edinburgh instrument company.
25. R. Czerwieniec, M. J. Leitl, H. H. H. Homeier, H. Yersin, *Coord. Chem. Rev.* 2016, **325**, 2–28.
26. R. Czerwieniec, J. Yu and H. Yersin, *Inorg Chem*. 2011, **50**, 8293–8301.
27. M. J. Leitl, D. M. Zink, A. Schinabeck, T. Baumann, D. Volz and H. Yersin, *Top Curr. Chem.* 2016, **374**, 25.
28. H. Yersin, A. F. Rausch, R. Czerwieniec, T. Hofbeck and T. Fischer, *Coord. Chem. Rev.* 2011, **255**, 2622–2652.
29. M.Wallesch, D. Volz, D. M. Zink, U. Schepers, M. Nieger, T.Baumann and S. Bräse, *Chem. Eur. J*. 2014, **20**, 6578−6590.
30. R. Czerwieniec, K. Kowalski and H. Yersin, *Dalton Trans*. 2013, **42**, 9826–9830.
31. X. L. Chen, R. M. Yu, Q. K. Zhang, L. J. Zhou, X. Y. Wu, Q. Zhang and C. Z. Lu, *Chem. Mater*. 2013, **25**, 3910–3920.
32. H.Ohara, A. Kobayashi and M. Kato, *Dalton Trans.* 2014, **43**, 17317–17323.
33. J. P. Launay and M. Verdaguer, *Electrons in Molecules: From Basic Principles to Molecular Electronics*. Oxford Univ. Press, UK, 2018.
34. J. B. Stothers, *Carbon-13 NMR spectroscopy* in Organic chemistry: A series of monographs. Elsevier, 2012.
35. M. T. Miller, P. K. Gantzel and T. B. Karpishin, *Inorg. Chem*. 1999, **38**, 3414–3422.
36. A. C. S. Samia, C. John, J. F. Christoph and B. Clemens, *J. Phys. Chem. B* 2004, **108**, 563−569.
37. X. K. Chen, D. Kim and J. L. Brédas, *Acc. Chem. Res.* 2018, **51**, 2215–2224.

ChemComm

COMMUNICATION

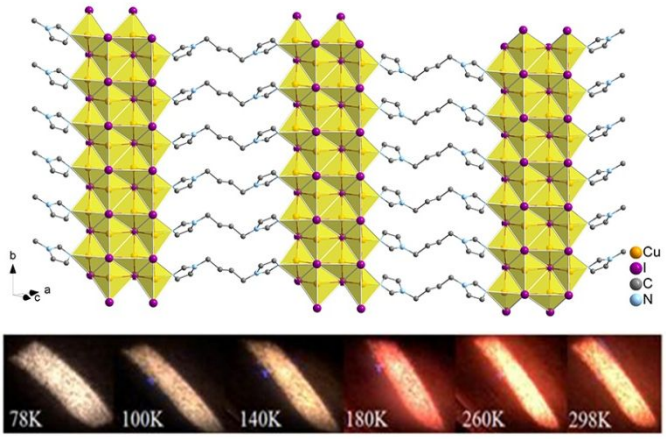

The work reports the observation of NTQ effect in a copper–organic framework emitter through delocalization–localization transition of its imidazole ligand.